Preparation of fibrous titania oxynitride – carbon catalyst and oxygen reduction reaction analysis in both acidic and alkaline media

Taro Kinumoto[*], Yoshinori Sou, Kohei Ono, Miki Matsuoka, Yasuhiko Arai, Tomoki Tsumura, Masahiro Toyoda

Department of Applied Chemistry, Faculty of Engineering, Oita University, 700 Dannoharu, Oita 870-1192, Japan

HIGHLIGHTS

- A fibrous catalyst of titania oxynitride and carbon is prepared.
- The catalyst works for the ORR in both $HClO_4$ and KOH aqueous solutions.
- The onset potential for the ORR is first determined at 0.95 V in KOH solution.
- The ORR mechanism in KOH solution is a peroxide intermediate pathway.

ARTICLE INFO

ABSTRACT

A fibrous catalyst of titania oxynitride and carbon is prepared and its catalytic behavior in the oxygen reduction reaction (ORR) are investigated in both $HClO_4$ and KOH aqueous solutions. TiO_2 particles are successfully deposited on activated carbon fibers by a liquid phase deposition technique using $(NH_4)_2TiF_6$ and H_3BO_3. The catalyst obtained after subsequent ammonia nitridation at 1273 K had a fibrous structure with TiO_xN_y and TiN components.

Interestingly, the product demonstrates catalytic activity for the ORR in not only $HClO_4$ but also KOH aqueous solution. The onset potential in $HClO_4$ solution is assumed to be moderate, at 0.85 V; on the other hand, that in KOH solution is relatively high at 0.95 V. Furthermore, it is considered from the Tafel plot analysis of the KOH solution result that the ORR mechanism follows a peroxide intermediate pathway and the rate-determining step would be a one-electron-transfer reaction to oxygen molecules adsorbed on the active site.

© 2014 Elsevier B.V. All rights reserved.

1. Introduction

Electrochemical power sources that use oxygen as a reactant will be indispensable for society's future energy needs. In particular, fuel cells, metal-air batteries, and hydrogen-air batteries are typical, and hold promise as the power sources for electric vehicles and stationary power generators [1–3].

However, challenges remain for the development of highly active catalysts (i.e., with low activation overpotentials) for oxygen electrode reactions, such as the oxygen reduction reaction (ORR; a discharge reaction) and oxygen evolution reaction (OER; a charge reaction). Despite over a century of catalyst exploration, Pt group elements and their alloys remain the most active electrode catalysts for the ORR, showing the lowest activation overpotentials in both acid and alkaline media [4–6].

Even with the best Pt-based electrode catalysts available, an overpotential exceeding 0.3 V is usually observed when an appreciable current for the ORR is generated in acidic as well as alkaline medium [4–6]. Furthermore, the low global abundance of Pt is also cause for concern. Use of Pt as an electrode catalyst remains a bottleneck for the realization of our clean energy goals. Therefore, an active electrode catalyst that can replace Pt, is highly abundant, and exhibits a low activation overpotential is being actively sought by many researchers.

The catalytic activity of titania oxynitride (TiO_xN_y) for the ORR in acidic aqueous solution was first reported by Ota et al. [7,8]. The natural abundance of Ti, O, and N is much higher than that of Pt. Recently, challenges for group 4 and 5 metal oxide-based catalysts

have also been carried out [9]. A carbon alloy has also shown promise for the ORR in acid solution [10]. Unfortunately, these materials exhibit insufficient catalytic activity, and Pt's current superiority makes it the most commonly used.

We are interested in the study of highly active ORR catalysts composed of abundant elements. Therefore, in this study, the preparation and catalytic properties of a titanium oxynitride-carbon (TiO_xN_y-C) catalyst with a fibrous morphology are reported. A fibrous structure affords higher power output in fuel cells because of superior gas diffusion properties [11,12]. The catalyst was prepared by loading TiO_2 particles on carbon fibers via a liquid phase deposition (LPD) technique followed by ammonia nitridation. Specifically, $(NH_4)_2TiF_6$ and H_3BO_3 were employed for TiO_2 loading on activated carbon fibers (ACF), in reference to the report by Y. Hou et al. [13]. Surprisingly, the TiO_xN_y-C obtained from ammonia nitridation at 1273 K showed the best catalytic activity for the electrochemical ORR in not only $HClO_4$ (acidic) but also KOH (alkaline) aqueous solution. The reaction mechanism is also discussed, and that for alkaline solution is elucidated for the first time, to the best of our knowledge. The findings of this study will motivate the further development of an active electrode catalyst that can replace Pt.

2. Experimental

2.1. Preparation and characterization of fibrous TiO_xN_y-C catalyst

Activated carbon fiber bundles (ACF, AD'ALL, A-10, UNITICA LTD., Brunauer–Emmett–Teller surface area = 1300 m^2 g^{-1}), cut to ~1 mm lengths, were employed as fibrous substrates for LPD. An aqueous solution of $(NH_4)_2TiF_6$ (0.05 mol dm^{-3}, Aldrich) was prepared in a polyethylene beaker. After complete dissolution of the titanate salt, H_3BO_3 (0.2 mol dm^{-3}, Kishida Chemical Co.) was added. ACF was immediately dispersed in the solution, the vessel was sealed with a plastic lid, and the reaction was stirred vigorously for 24 h. The sample was collected by vacuum filtration, mounted in an alumina boat, and heat treated in an electric tube furnace at 1273 K for 1 h under Ar.

Subsequent ammonia nitridation was carried out in an electric tube furnace equipped with a quartz glass tube under flowing ammonia (Iwatani, 99.9%) at 1233 K for 2 h. The heating rate was 5 K min^{-1}, and nitrogen gas was flowed up to 373 K.

X-ray diffraction patterns (XRD; Rigaku, Geigerflex) were obtained before and after nitridation to investigate the composition and crystalline phase. The structure of the products was observed by field-emission scanning electron microscopy (FE-SEM; JEOL, JSM-6701F). The elemental composition was analyzed by energy dispersive X-ray spectroscopy (EDS; JEOL, JED-2300) in conjunction with FE-SEM. Thermogravimetric analysis was carried out using a TG-DTA system (Rigaku, TG8120) under atmospheric air up to 1273 K. The amount of TiO_2 deposited by LPD was estimated from the residual weight after combustion of the ACF. The detailed chemical state of the product after nitridation was investigated by using X-ray photoelectron spectroscopy (XPS; ULVAC-PHI, PHI5000 VersaProbe).

### 2.2. Electrochemical oxygen reduction reaction study

A rotating disk electrode (RDE) technique is generally employed to investigate intrinsic catalytic activity in the ORR among candidate catalysts. We applied the method proposed by T. J. Schmidt et al. to evaluate the catalytic activity of our catalyst in the ORR [14,15]. The product was ultrasonically dispersed in an aqueous solution containing ethanol and applied dropwise to a polished glassy carbon disk (Tokai Carbon) or a Ti metallic disk (Nilaco Corp.)

for use in acidic or alkaline solutions, respectively. The disk diameters were 5 mm. The catalyst loading on each disk electrode was 100 μg. To measure the ORR activity in acidic medium, a thin Nafion film was formed on the working electrode by casting the corresponding ionomer (Aldrich). In contrast, the anion exchange ionomer AS-4 (Tokuyama Corp.) was used for the activity measurements in alkaline medium. The calculated thicknesses of the Nafion and AS-4 layers were controlled to 80 nm. For the acidic medium studies, a glass electrochemical cell was employed, and aqueous $HClO_4$ solution (0.1 mol dm^{-3}, Kanto Chemical Co.), a reversible hydrogen electrode (RHE), and Au mesh were used as the electrolyte, reference electrode, and counter electrode, respectively. For the alkaline medium, the electrochemical cell was made of polytetrafluoroethylene. Aqueous KOH solution (0.1 mol dm^{-3}, Kishida), an Hg/HgO electrode, and Ni mesh were employed as the electrolyte, reference electrode, and counter electrode, respectively. The potential is given vs. the RHE. Electrochemical measurements were performed at 298 K with a potentiostat (ALS, model 700B). The current per unit weight of the sample (mass current density; A g^{-1}) obtained under N_2 atmosphere (i_N) subtracted from that under O_2 atmosphere (i_O) was assumed to be responsible for the ORR. An AFMSRCE rotator (Pine Research Instrumentation) was used for the RDE.

3. Results and discussion

3.1. Characterization of fibrous TiO_xN_y-C catalyst

The XRD pattern of the resultant material after LPD-TiO_2 deposition is shown in Fig. 1a). A broadened diffraction peak between $2\theta = 20$ and $25°$ is assigned to the amorphous carbon structure originating from the ACF. A large diffraction peak corresponding to the highest peak assigned to anatase TiO_2 (JCPDS No. 00-021-1272) only appears at $2\theta = 25.28°$, clearly showing the formation of TiO_2 by the LPD. Unfortunately, the other diffraction peaks corresponding to anatase TiO_2 were not clearly visible. This may be related to not only the low crystallinity of the TiO_2 as prepared, but also the low TiO_2 content (9 wt%), as estimated by thermogravimetric analysis-differential thermal analysis (TG-DTA) of the product. The sharp peak at $2\theta = \sim27.48°$ indicates rutile TiO_2. Interestingly, the anatase TiO_2 crystal structure persists even after heat treatment at 1273 K; the anatase-to-rutile phase transition in
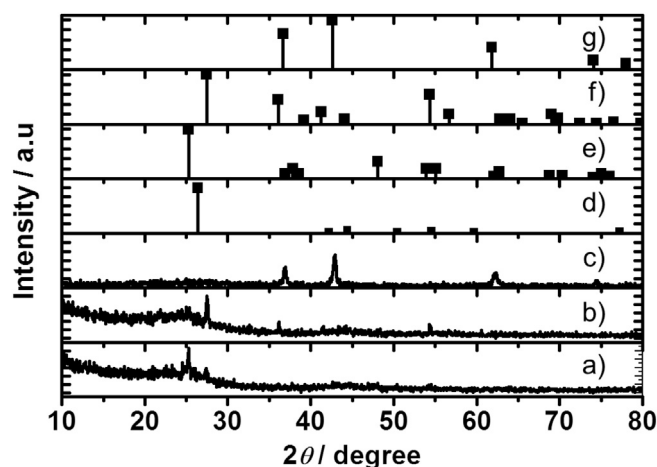
Fig. 1. X-ray diffraction patterns of the product a) after LPD-TiO_2 deposition, and after subsequent ammonia nitridation at b) 973 K and c) 1233 K. Standard patterns for d) graphite (JCPDS 00-041-1487), e) anatase TiO_2 (JCPDS 00-021-1272), f) rutile TiO_2 (JCPDS 00-021-1276) and g) TiN (JCPDS 00-038-1420).
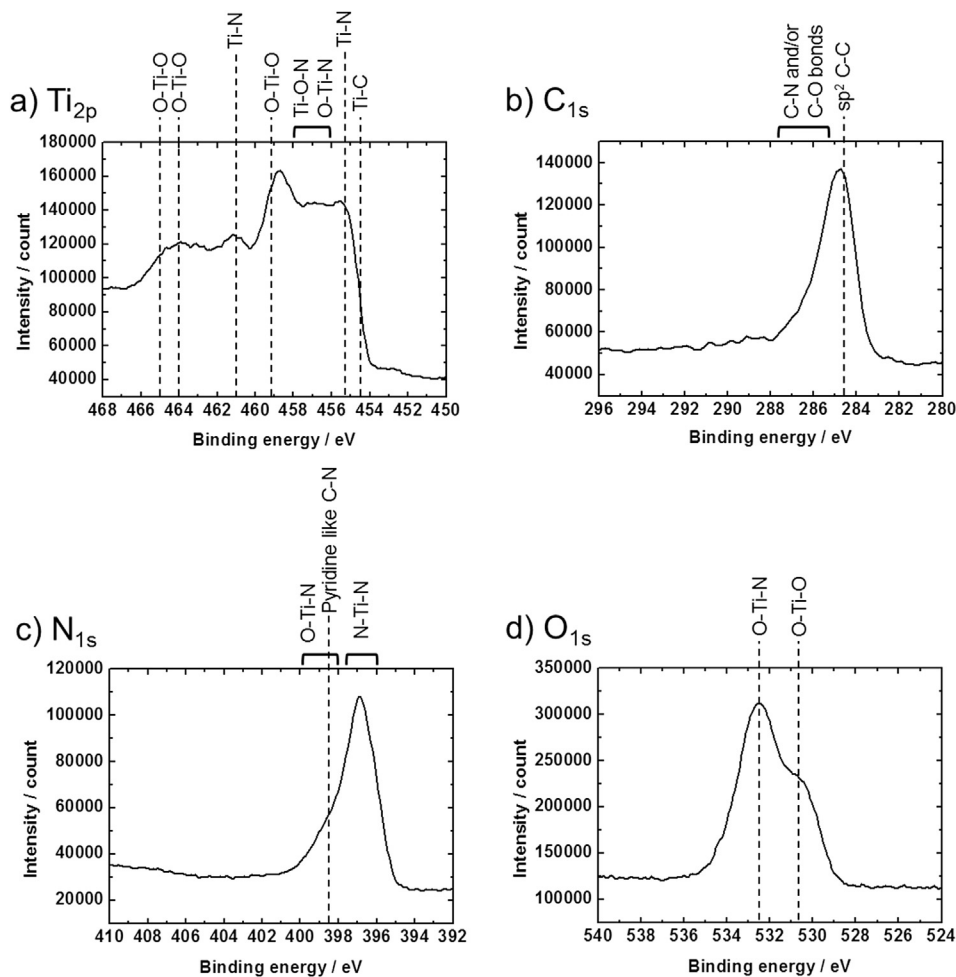
Fig. 2. X-ray photoelectron spectra of the product: a) Ti_{2p}, b) C_{1s}, c) N_{1s}, and d) O_{1s}.

TiO_2 typically takes place when heated above 1188 K under inert atmosphere. Although the reasons for this remain unclear at present, ACF likely behaves as an inhibitor for the TiO_2 phase transition.

The reactions for the formation of TiO_2 during LPD are theoretically considered as follows [16—18]. TiO_2 can be formed by hydrolysis of the TiF_6^{2-} complex, as in Equation (1). The reaction is driven toward TiO_2 formation in the presence of boric acid since fluoride anion is consumed by the formation of BF_4^- [Equation (2)].

$$TiF_6{}^{2-} + 2H_2O \rightleftharpoons TiO_2 + 6F^- + 4H^+ \tag{1}$$

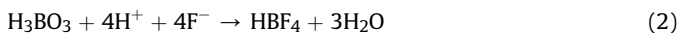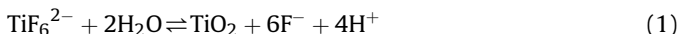$$H_3BO_3 + 4H^+ + 4F^- \rightarrow HBF_4 + 3H_2O \tag{2}$$

Fig. 1b) shows the XRD pattern of the product after nitridation at 973 K. A large broadened peak assigned to graphite remained even after the heat treatment. In addition, a sharp peak due to rutile TiO_2 was observed at $2\theta = {\sim}27.48°$, $36.09°$ and $54.32°$. As shown in Fig. 1c), the diffraction peaks derived from TiO_2 and ACF disappear, and several peaks assigned to TiN are observed after ammonia nitridation at 1233 K for 2 h. This result is consistent with those reported by Chisaka et al., who showed that XRD peaks corresponding to the TiN phase were mainly found after the ammonia nitridation of titanium carbonitride ($TiC_{0.82}N_{0.23}O_{0.06}$) over 3 h at 1073 K, whereas peaks attributable to rutile TiO_2 were mainly observed below 973 K [19].

Similar results were observed in our study, as shown in Fig. 1b) and c). In fact, after the ammonia nitridation was carried out at 973 K, residual rutile TiO_2 and the absence of the TiN phase were confirmed by XRD measurement [Fig. 1b)], which clearly shows that nitridation did not take place below this temperature. Thus, it is reasonable to consider, as reported by Chisaka et al., that the nitridation degree (as indicated by the appearance of the TiN phase) is dependent on the ammonia nitridation temperature [19]. On the other hand, if the ammonia nitridation temperature was higher than 1233 K, the ACF would be severely decomposed and the products would be unable to fully retain a fibrous structure.

The presence of O—Ti—O, Ti—N, Ti—O—N, and O—Ti—N bonding was evident in the Ti_{2p} XPS spectrum of the product at 1233 K. The Ti_{2p}, C_{1s}, N_{1s}, and O_{1s} spectra are shown in Fig. 2. Each peak was identified based on the literature [20—26]. The appearance of Ti—O—N and O—Ti—N bonding in the Ti_{2p} spectrum clearly indicates the formation of TiO_xN_y. Although we have not yet been able to measure the nitrogen content, some portion of TiO_2 was likely converted to TiN by nitridation, as reported by Chisaka et al. [19]. A peak fraction presumably attributable to pyridine-like C—N bonding is observed in the N_{1s} spectrum; however, its formation cannot be confirmed in the C_{1s} spectrum because of the overlap of the peaks assigned to several kinds of C and O bonding modes [25]. Nevertheless, the N_{1s} spectrum strongly suggests that pyridine-type C—N bonds are formed during ammonia nitridation [26]. The atomic ratio of C, N, O, and Ti after nitridation at 1233 K was

measured by EDS as 35:46:15:4. The relatively high nitrogen composition should correspond to the formation of the TiN phase that was introduced to the ACF, which would lead to the formation of C−N bonding. Carbon was also probably introduced into the titania oxynitride layer during ammonia nitridation and would influence the ORR activity; unfortunately, it is hardly possible to measure the carbon content due to its low abundance as well as the ACF remaining after the nitridation [Fig. 3].

An FE-SEM image of the sample after LPD [Fig. 3a)] shows that TiO_2 particles were thickly deposited on the ACF surface. In addition, particles of several hundred nanometers in size were observed. Fig. 3b) shows the FE-SEM image of the lateral face of the product after ammonia nitridation at 1233 K. The fibrous morphology with the precipitates on the surface is recognizable as "pyrrosia piloselloides". The fibers with the surface-bound precipitates resemble fine lace, forming not only a network structure but also a large number of pores. These may allow the rapid diffusion of reactants, and increase the active surface area inside the catalyst [11,12]. The edge face is shown in Fig. 3c). The ACF remains as a core even after the heat treatment, although the weight of the ACF was reduced and its diameter decreased by ca. 50%. The reduction in weight as well as diameter suggests decomposition of the ACF during ammonia nitridation.

3.2. Hydrodynamic voltammograms in $HClO_4$ and KOH aqueous solutions

In Fig. 4, the solid line "a)" shows the voltammogram for the ORR in $HClO_4$ solution obtained at 1600 rpm. An enlargement of the region between 0.6 and 1.0 V is shown in the lower panel. An appreciable reduction current was observed below ca. 0.85 V in the voltammogram, demonstrating that the product has intrinsic catalytic activity for ORR in $HClO_4$ solution.

Surprisingly, the product also catalyzes the ORR in KOH solution. The dashed line "b)" shows the hydrodynamic voltammogram of the product in alkaline medium. A high onset potential approaching that of Pt was determined by the appreciable reduction current after 0.95 V [27]. Ohnishi et al. investigated the ORR activity of TiN
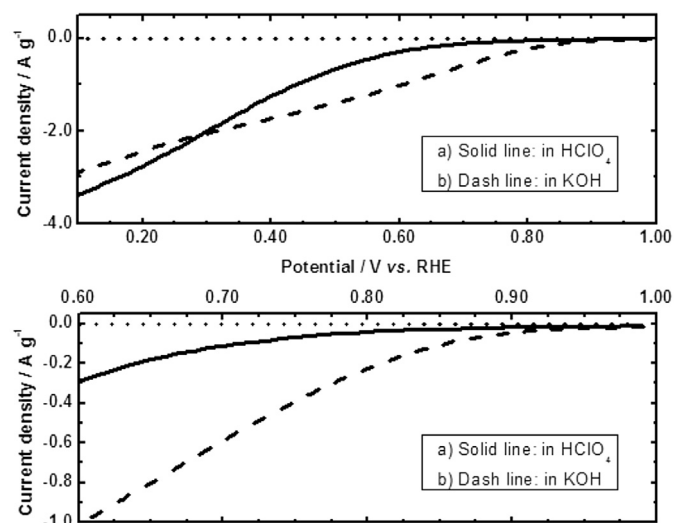

Fig. 4. Hydrodynamic voltammograms of the product in a) $HClO_4$ (solid line) and b) KOH (dashed line) aqueous solutions (upper). Enlargement of the 0.6−1.0 V region (lower).

nanoparticles in 0.1 mol dm^{-3} NaOH solution [28], and found an onset potential of 0.85 V vs. RHE for the prepared TiN nanoparticles, although commercial TiN (>100 nm in size) did not exhibit activity. To the best of our knowledge, the number of ORR studies for titania analogs in alkaline vs. acidic media is limited, and studies concerned with kinetics and mechanism are especially rare. In the following section, we attempt a detailed discussion of the ORR mechanism of our catalyst.

3.3. Discussion of the oxygen reduction reaction in $HClO_4$ aqueous solution

In electrochemical kinetics, the Tafel equation relates the current of an electrochemical reaction to the overpotential (η), as given by.
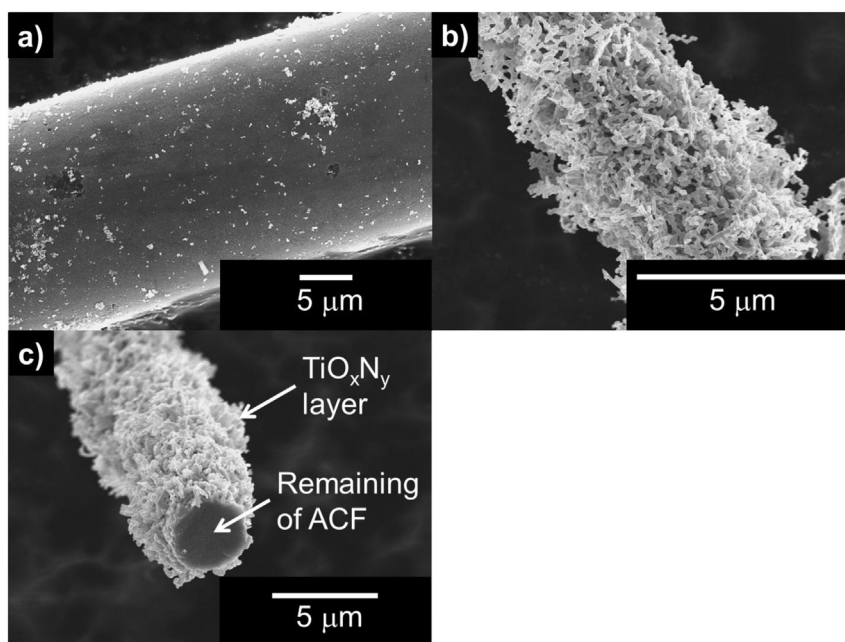

Fig. 3. FE-SEM images of the product a) after LPD-TiO_2 deposition. b) Lateral and c) edge faces after subsequent ammonia nitridation.

$$\eta = a + b \log i_d \qquad (3)$$

Here, a, b, and i_d are the Tafel constant, the slope, and the current density, respectively. The slope is considered in this study since it provides information about the reaction mechanism and identifies the rate-determining step of the overall reaction. The Tafel equation enables the estimation of the kinetic parameters for the ORR when the overpotential is below 1.102 V, since the theoretical potential is 1.22 V.

The *iR*-corrected Tafel plots for the $HClO_4$ solution are shown in Fig. 5a). The slope is ~240 mV dec^{-1} in the 0.9–0.65 V range, in good agreement with that reported for the reduction of H_2O_2 on a gold electrode [29]. The cathodic ORR is well known as a multi-electron reaction associated with the formation of reaction intermediates. The most commonly considered reaction mechanism was proposed by Damjanovic et al. [6]. When the voltammetry experiment is performed in the anodic direction from 0.05 to 1.0 V, H_2O_2 would be produced at a potential below 0.67 V vs. SHE according to.

$$O_2 + 2H^+ + 2e^- \rightarrow H_2O_2 \qquad (4)$$

and then further reduced and/or decomposed to water.

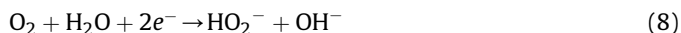$$H_2O_2 + 2H^+ + 2e^- \rightarrow 2H_2O \qquad (5)$$

Therefore, in this case, the mechanism of ORR is considered to include reactions (4) and (5) rather than a direct four electron reaction as reported for Pt in acidic medium [Equation (6)].

$$O_2 + 4H^+ + 4e^- \rightarrow 2H_2O \qquad (6)$$

In theory, H_2O_2 is not thermodynamically produced above 0.67 V vs. RHE. Thus, to investigate the activity for the direct four electron transfer pathway [Equation (6)], the Tafel slope was obtained above 0.70 V from the voltammogram in the cathodic direction [Fig. 5a), circle symbols]. The slope, ~158 mV dec^{-1} in the 0.85–0.70 V range, is larger than that of Pt (60 and 120 mV dec^{-1} for lower and higher overpotential regions, respectively) and suggests (unfortunately) a lower catalytic activity [4–6]. The lower ORR activity of our product might be the result of physicochemical properties such as low crystallinity and low surface area, or even the formation of a large TiN phase [19,30]. Improvement in the catalytic activity might be achieved by optimization of the mass fraction of active sites, which is a key feature in determining ORR activity [19,30].

3.4. Discussion of the oxygen reduction reaction in KOH aqueous solution

The *iR*-corrected Tafel plots for the KOH medium are shown in Fig. 5b). The plots exhibit two different slopes, −123 and −239 mV dec^{-1} at 0.95–0.8 V and 0.8–0.65 V, respectively. The larger slope may involve the mass transport of oxygen. The mechanism for the ORR can be elucidated as either a direct four-electron pathway [Equation (7)] or a peroxide intermediate pathway [Equations (8) and (9)] [4–6].

$$O_2 + 4H^+ + 4e^- \rightarrow 4OH^- \qquad (7)$$

$$O_2 + H_2O + 2e^- \rightarrow HO_2^- + OH^- \qquad (8)$$

$$HO_2^- + H_2O + 2e^- \rightarrow 3OH^- \qquad (9)$$

Equation (7) was proposed as the mechanism for a Pt-mediated reaction in which the Tafel slope was reported as 60 mV dec^{-1} [4–6,27]. The mechanism that includes Equations (8) and (9) has been proposed for graphite (and most carbonaceous materials), gold, most oxide-covered metals (Ni, Co), most transition metal oxides, and transition metal macrocycles [4,5]. In the case of gold and stress-annealed pyrolitic graphite, the Tafel slope was 120 mV dec^{-1}, which is very close to our result in the 0.95–0.8 V region [4–6]. Even though it is difficult to determine the reaction mechanism from only the Tafel slope, the ORR mechanism in alkaline solution is not likely to be the direct four-electron pathway, but rather, the peroxide intermediate pathway. Therefore, the rate-determining step of the ORR for our catalyst in KOH solution is assumed to be [4–6],

$$O_{2(ads)} + e^- \rightarrow O_{2(ads)}^{\cdot-} \qquad (10)$$

where (ads) indicates "adsorption at the active site". Equation (11) should follow:

$$2O_{2(ads)}^{\cdot-} + H_2O \rightarrow O_2 + HO_2^- + OH^- \qquad (11)$$
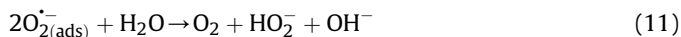
In turn, the onset potential for the ORR should be determined at 0.95 V, as the curve has a reasonable slope there in the Tafel plots.

In this study, we prepared an electrode catalyst with a fibrous, porous morphology via the LPD of TiO_2 on ACF followed by heat treatment and ammonia nitridation. As determined by the onset potential, the catalyst shows ORR activity in both acid and alkaline media, and approaches that of Pt in the latter. This catalyst contains only the highly abundant elements C, O, N, and Ti, which will reduce both the costs and material limitations of the electrochemical power sources that use oxygen as a reactant. Although the present catalytic activity of our product for the ORR is insufficient,
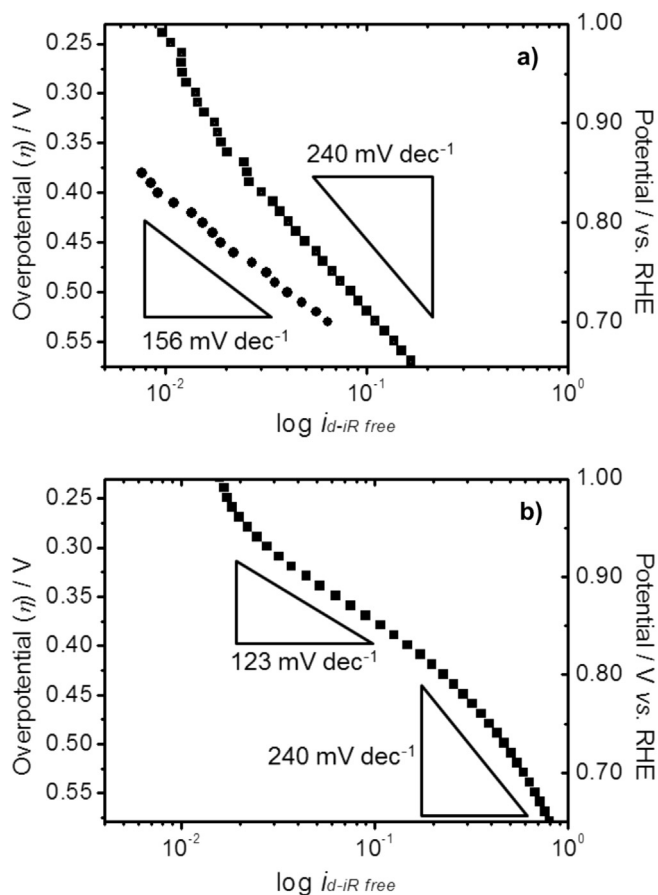

Fig. 5. Tafel plots of the product in a) $HClO_4$ and b) KOH aqueous solutions. Square and circle symbols in a) show plots obtained in the anodic and cathodic voltammetry directions.

we expect that further studies of its active sites, crystallinity, and surface area will afford significant improvement.

4. Conclusion

A fibrous catalyst composed of titania oxynitride and activated carbon fibers (TiO_xN_y-C) was prepared and its catalytic activity and the reaction mechanism for the ORR were investigated in both $HClO_4$ (acidic) and KOH (alkaline) solutions.

The results of the XRD and XPS analyses revealed the formation of TiO_xN_y and TiN. In particular, O–Ti–O, Ti–N, Ti–O–N, and O–Ti–N bonds were recognized by XPS. FE-SEM observation revealed a fibrous morphology with a networked structure of precipitates on the fiber surface and a large number of internal pores.

The RDE study showed that the prepared TiO_xN_y-C catalyzes the ORR in both $HClO_4$ and KOH aqueous solutions. The onset potential in $HClO_4$ solution is assumed to be moderate at 0.85 V. On the other hand, the onset potential for the ORR was determined, for the first time, to be at 0.95 V in KOH solution, where the curve has a reasonable slope in the Tafel plot, and which surprisingly approximates that of Pt. Furthermore, it is considered from the Tafel plot analysis that the ORR mechanism in KOH solution follows a peroxide intermediate pathway and the rate-determining step would be a one-electron transfer to oxygen molecules adsorbed at the active site.

Acknowledgments

References

[1] N. Imanishi, O. Yamamoto, Mater. Today 17 (2014) 24–30.
[2] M. Winter, R.J. Brodd, Chem. Rev. 104 (2004) 4245–4269.
[3] M. Morimitsu, T. Kondo, K. Takano, Electrochem 5 (2010) 493–496.
[4] K. Kinoshita, Electrochemical Oxygen Technology, John Wiley & Sons, Inc, 1992, pp. 19–40.
[5] E. Yeager, Electrochim. Acta 29 (1984) 1527–1537.
[6] A. Damjanovic, M. Genshaw, J. Bockris, J. Phys. Chem. 70 (1966) 3761–3762.
[7] J.H. Kim, A. Ishihara, S. Mitsushima, N. Kamiya, K. Ota, Electrochim. Acta 52 (2007) 2492–2497.
[8] Y. Ohgi, A. Ishihara, Y. Shibata, S. Mitsushima, K. Ota, Chem. Lett. 37 (2008) 608–609.
[9] K. Ota, Y. Ohgi, K.D. Nam, K. Matsuzawa, S. Mitsushima, A. Ishihara, J. Power Sources 196 (2011) 5256–5263.
[10] F. Jaouen, J. Herranz, M. Lefevre, J.P. Dodelet, U.I. Kramm, I. Herrmann, P. Bogdanoff, J. Maruyama, T. Nagaoka, A. Garsuch, J.R. Dahn, T. Olson, S. Pylypenko, P. Atanassov, E.A. Ustinov, ACS Appl. Mater. Interfaces 1 (2009) 1623–1639.
[11] M.K. Debe, A.K. Schmoeckel, G.D. Vernstrom, R. Atanasoski, J. Power Sources 161 (2006) 1002–1011.
[12] S. Murata, M. Imanishi, S. Hasegawa, R. Namba, J. Power Sources 253 (2014) 104–113.
[13] Y. Hou, J. Qu, X. Zhao, P. Lei, D. Wan, C.P. Huang, Sci. Total Environ. 407 (2009) 2431–2439.
[14] T.J. Schmidt, H.A. Gasteiger, G.D. Stab, P.M. Urban, D.J. Kolb, R.J. Behm, J. Electrochem. Soc. 145 (1998) 2354–2358.
[15] U.A. Paulus, T.J. Schmidt, H.A. Gasteiger, R.J. Behm, J. Electroanal. Chem. 495 (2001) 134–145.
[16] S. Deki, N. Yoshida, Y. Hiroe, K. Akamatsu, M. Mizuhata, A. Kajinami, Solid State Ionics 151 (2002) 1–9.
[17] S. Deki, S. Iizuka, M. Mizuhata, A. Kajinami, J. Electroanal. Chem. 584 (2005) 38–43.
[18] T. Kinumoto, K. Nagano, Y. Yamamoto, T. Tsumura, M. Toyoda, J. Power Sources 249 (2014) 503–508.
[19] M. Chisaka, A. Ishihara, K. Suito, K. Ota, H. Muramoto, Electrochim. Acta 88 (2013) 697–707.
[20] K.S. Robinson, P.M.A. Sherwood, Surf. Interface Anal. 6 (1984) 261–266.
[21] N.C. Saha, H.G. Tompkins, J. Appl. Phys. 72 (1992) 3072–3079.
[22] X. Chen, C. Burda, J. Phys. Chem. B 108 (2004) 15446–15449.
[23] Y. Cong, J. Zhang, F. Chen, M. Anpo, J. Phys. Chem. C 111 (2007) 6976–6982.
[24] B. Avasarala, T. Murray, W. Li, P. Haldar, J. Mater. Chem. 19 (2009) 1803–1805.
[25] H. Choo, T. Kinumoto, S.K. Jeong, Y. Iriyama, T. Abe, Z. Ogumi, J. Electrochem. Soc. 154 (2007) B1017–B1023.
[26] E. Raymundo-Piñero, D. Cazorla-Amorós, A. Linares-Solano, J. Find, U. Wild, R. Schlögl, Carbon 40 (2002) 597–608.
[27] F.H.B. Lima, J. Zhang, M.H. Shao, K. Sasaki, M.B. Vukmirovic, E.A. Ticianelli, R.R. Adzic, J. Phys. Chem. C 111 (2007) 404–410.
[28] R. Ohnishi, M. Katayama, D. Cha, K. Takanabe, J. Kubota, K. Domen, J. Electrochem. Soc. 160 (2013) F501–F506.
[29] R. Zeis, T. Lei, K. Sieradzki, J. Snyder, J. Erlebacher, J. Catal. 253 (2008) 132–138.
[30] M. Chisaka, A. Ishihara, K. Ota, H. Muramoto, Electrochim. Acta 113 (2013) 735–740.